A Compact Dual-Resonant Terahertz MIMO Antenna for 6G Communications

Md. Ashraful Haque
Department of Electrical and Electronic Engineering, Daffodil International University, Dhaka, Bangladesh
limon.ashraf@gmail.com (corresponding author)

Maruf Billah
Department of Electrical and Electronic Engineering, Daffodil International University, Dhaka, Bangladesh
billah33-1773@diu.edu.bd

Jun-Jiat Tiang
Centre for Wireless Technology, CoE for Intelligent Network, Faculty of Artificial Intelligence and Engineering, Multimedia University, Persiaran Multimedia, Cyberjaya, Selangor, Malaysia
jjtiang@mmu.edu.my (corresponding author)

Narinderjit Singh Sawaran Singh
Faculty of Data Science and Information Technology, INTI International University, Persiaran Perdana BBN, Putra Nilai, Negeri Sembilan, Malaysia
narinderjits.sawaran@newinti.edu.my

Mahafujul Haq Riad
Department of Electrical and Electronic Engineering, Daffodil International University, Dhaka, Bangladesh
riad33-1728@diu.edu.bd

Received: 12 December 2025 | Revised: 15 January 2026, 7 February 2026, and 27 February 2026 | Accepted: 4 March 2026

 DOI: https://doi.org/10.48084/etasr.16909

ABSTRACT

The increasing demand for ultra-high data rates and extensive connectivity in sixth-generation (6G) networks positions terahertz (THz) frequencies as a crucial facilitator. This work presents a compact, high-performance Multiple-Input Multiple-Output (MIMO) antenna for THz applications, with a remarkable 1.83 THz bandwidth and twin resonances at 4.73 THz and 5.47 THz. The antenna demonstrates exceptional performance, featuring a high gain of 13.15 dB, a radiation efficiency of 91.33%, and an isolation of −31.41 dB. This design introduces a notable advancement through the integration of an RLC circuit model, which provides validation of the proposed design. The antenna exhibits a remarkable Diversity Gain (DG) of 9.9988 dB and a negligible Envelope Correlation Coefficient (ECC) of 0.00027. Its compact dimensions (90 × 205 μm²) and copper–polyimide composition render it an optimal choice for forthcoming 6G communications, THz imaging, and sensing applications.

Keywords-terahertz (THz); microstrip antenna; MIMO; dual resonance; industrial and innovation

I. INTRODUCTION

The emergence of sixth-generation (6G) wireless communication extends beyond connectivity; it is a new modality for interacting with technology and the environment [1]. Enhancing current network functionalities, 6G has the potential to provide expedited speeds and more reliable links, leading to an era of real-time, high-bandwidth applications [2]. For example, in virtual reality, 6G will facilitate the transmission of massive amounts of information at speeds that can provide seamless, high-quality experiences without any interruptions [3]. The ubiquitous, low-latency nature of 6G will also be indispensable for autonomous systems such as cars and drones, which demand high performance [4]. With the

associated growth of the Internet of Everything (IoE), 6G is set to connect a vast number of interconnected devices.

Exploitation of the terahertz (THz) frequency band (0.1–10 THz) [5] is one of the fundamental enablers for fully realizing the capabilities of 6G. This wide bandwidth can be considered a potential spectrum resource to meet the high data rate and massive capacity requirements of 6G networks [6]. Multi-gigabit-per-second data transmission with ultra-low latency can be achieved at THz frequencies, which is essential for futuristic applications such as remote surgery, real-time holographic communications, and high-precision manufacturing [7, 8].

The challenges associated with fully enabling 6G in the THz band include the design of power-efficient, high-gain antennas. THz frequencies combined with Multiple-Input Multiple-Output (MIMO) techniques offer significant advantages, such as higher capacity, improved signal quality, and extended coverage [9]. Multiple antennas are used in MIMO systems at both the transmitter and the receiver to generate multiple independent channels, thereby increasing channel capacity [10]. It is also necessary to enhance the performance of THz MIMO antennas to fully exploit the potential of 6G. Such antennas are essential for delivering ultra-fast, massive, low-latency, and highly dependable connectivity across various use cases. In terms of antenna technology [11], recent developments in THz antennas are expected to drive a revolution in wireless communication and transform how people connect and communicate as the digital era advances [12].

The progress of THz communications and MIMO antennas has been thoroughly reviewed in recent literature, emphasizing their key roles in 6G development. Unlike previously reported results, the proposed antenna demonstrates a wider bandwidth, higher gain, better isolation, higher efficiency, and improved Diversity Gain (DG), and can be integrated with RLC components. The prototype in [13] operates at 0.445 and 0.540 THz with bandwidths of 0.021 THz and 0.036 THz, respectively. Although it has a 7.9 dB gain and 85.64% efficiency, its low mutual decoupling (less than −20 dB) and high Envelope Correlation Coefficient (ECC) of 0.075 degrade MIMO performance. The large (39.28 λ_o × 25.24 λ_o) size prevents compact system integration. This configuration has low gain, narrow bandwidth, and moderate isolation; it performs poorly at high frequencies.

The antenna presented by authors in [14] achieves resonance at 0.395 THz and 0.629 THz with bandwidths of 0.01 THz and 0.025 THz, respectively. Although it achieves high efficiency (92.48%) and isolation (−20 dB), the gain is low (5.17 dB), and its large size (15.77 λ_o × 18.93 λ_o) limits its use in high-performance THz systems. Authors in [15] presented a 0.128 THz and 0.178 THz resonant antenna with very narrow bandwidths of 0.004 THz and 0.0061 THz, respectively. Wideband THz applications for such designs appear limited due to bandwidth constraints; however, very good isolation (−25 dB), high efficiency (90%), and excellent DG (9.999 dB) were achieved without RLC complexity. The absence of an RLC model limits the system's ability to maintain performance under varying operating conditions.

Authors in [16] presented an antenna designed for 0.472 THz with a bandwidth of 0.435 THz. Although the antenna achieves a good DG (9.99 dB) and isolation (−20 dB), it suffers from low gain (3.9 dB) and high ECC (0.458) due to strong inter-element correlation. Its large footprint (9.46 λ_o × 4.73 λ_o) also limits compact integration. The absence of an RLC model further affects resonance stability. Authors in [17] reported operation at 0.654 THz, achieving a high gain of 11.3 dB, isolation of 25 dB, and excellent diversity performance (ECC: 0.003, DG: 9.99 dB) with a narrow bandwidth of 0.04 THz. However, its low efficiency (76.45%) and large footprint (18.93 λ_o × 34.71 λ_o) limit its applicability in compact systems.

Authors in [18] presented an antenna that operates at 0.514 THz with a bandwidth of 0.4 THz. It achieves high isolation (−25 dB), an efficiency of 85.24%, and a DG of 9.99 dB. Nevertheless, its relatively modest gain of 5.49 dB, size of (9.46 λ_o × 4.73 λ_o), and coupling (ECC: 0.015) constrain its performance in compact, high-performance MIMO applications. With the addition of RLC, the design could be greatly improved to be more robust against resonance losses, resulting in improved performance and stability.

Authors in [19] presented an antenna operating at 7.5 THz with a small footprint (1.57 λ_o × 1.57 λ_o) and a wide bandwidth of 5.9 THz. It achieves a DG of 9.97 dB and an ECC of 0.005, but suffers from low isolation (−16 dB) and moderate gain (8.3 dB), limiting its applicability in high-performance systems. Authors in [20] presented an antenna operating at 3.3 THz, 3.7 THz, and 3.9 THz with a bandwidth of 1.25 THz. It achieves gain of 10 dB, isolation above 20 dB, and ECC ≤ 0.005. However, the absence of RLC modeling and small board size (1.89 λ_o × 2.83 λ_o) limits resonance control, especially at high frequencies.

The antenna proposed by authors in [21] operates at 2.2 THz with 0.78 THz bandwidth and gain of 4.4 dB. Despite 92% efficiency, its −20 dB isolation limits performance. Its small size ensures minimal signal interference, as indicated by the antenna's dimensions (1.57 λ_o × 1.65 λ_o), DG of 9.99 dB, and ECC of 0.006. However, it is not appropriate for contemporary applications that require faster performance and wider bandwidth due to its low gain and limited bandwidth. Its overall performance could be enhanced by adding RLC components, particularly at higher frequencies, and resonance-related problems could be reduced.

The design in [22] operates at 2.8 THz with a 1.5 THz bandwidth with a small board size (1.57 λ_o × 1.57 λ_o). However, it lacks RLC validation. Authors in [23] proposed an antenna operating at 1.89 THz with 1.59 THz bandwidth and low gain of 4.6 dB. The antenna has a moderate isolation of −25 dB and a low efficiency of 74.5%. It guarantees good signal integrity with a DG of 10 dB and an ECC of $\leq 10^{-10}$ and its small board size (0.59 λ_o × 0.39 λ_o). However, its lack of RLC and low gain limits its ability to address resonance issues, particularly at higher frequencies.

Authors in [24] reported multiple resonances with very narrow bandwidths (0.036, 0.043, 0.06 THz), low gain (>5 dB), low efficiency (>60%), and isolation above −15 dB. The antenna ensures signal integrity with a DG of 9.99 and an ECC

of <0.02, featuring a compact board size (0.78 $\lambda_o \times 0.63\ \lambda_o$). Its low isolation, low gain, low efficiency, and narrow bandwidth make it less capable, especially at high frequencies, and validation is lacking without RLC assistance.

The proposed antenna demonstrates a remarkable performance improvement, covering 4.73 THz and 5.47 THz at multiple resonances with a bandwidth of 1.83 THz. The architecture achieves Ultra-Wideband (UWB) performance beyond conventional bandwidth limitations. A high gain of 13.15 dB and efficiency of 91.33% indicate strong radiation performance. The proposed architecture achieves isolation of −31.41 dB, greatly suppressing interference. An ECC of 0.00027 and a DG of 9.9988 dB ensure superior MIMO performance. The antenna differs from existing designs through the use of RLC components, leading to improved tunability and reduced resonance-related losses. RLC components ensure that the antenna maintains stable performance over a wide frequency range and that signal attenuation caused by frequency variation is effectively suppressed. The compact board size (1.419 $\lambda_o \times 3.78\ \lambda_o$) facilitates integration into compact systems. The design provides an effective solution for future-generation THz communication systems with its wide bandwidth, high gain, strong isolation, and RLC components. Table I compares various MIMO antenna configurations in terms of bandwidth, isolation, gain, efficiency, ECC, DG, and the inclusion of RLC circuits. The proposed antenna demonstrates improved performance compared to existing designs.

TABLE I. PERFORMANCE COMPARISON OF THE PROPOSED ANTENNA WITH EXISTING DESIGNS

Ref.	Resonance (THz)	BW (THz)	Gain (dB)	Efficiency (%)	Isolation (dB)	ECC	DG (dB)	Substrate material	Board size	MIMO configuration	RLC
[13]	0.445, 0.540	0.021, 0.036	7.9	85.64	−20	0.07	0.975	Polyimide	39.28 $\lambda_o \times 25.24\ \lambda_o$	4×4	Yes
[14]	0.395, 0.629	0.01, 0.025	5.17	92.48	−20	0.0125	10	Polyimide	15.77 $\lambda_o \times 18.93\ \lambda_o$	4×4	Yes
[15]	0.128, 0.178	0.004, 0.0061	6.24	90	−25	0.012	9.999	Polyimide	42.59 $\lambda_o \times 57.58\ \lambda_o$	2×2	No
[16]	0.472	0.435	3.9	79.16	−20	0.458	9.99	Polyimide	9.46 $\lambda_o \times 4.73\ \lambda_o$	1×2	No
[17]	0.654	0.04	11.3	76.45	≥25	0.003	9.99	Polyimide	18.93 $\lambda_o \times 34.71\ \lambda_o$	2×4	No
[18]	0.514	0.4	5.49	85.24	−25	0.015	9.99	Polyimide	9.46 $\lambda_o \times 4.73\ \lambda_o$	1×2	No
[19]	7.5	5.9	8.3	–	−16	0.005	9.97	SiO_2	1.57 $\lambda_o \times 1.57\ \lambda_o$	2×2	Yes
[20]	3.3, 3.7, 3.9	1.25	10.8	>80	>20	≤0.005	10	SiO_2	1.89 $\lambda_o \times 2.83\ \lambda_o$	1×2	No
[21]	2.2	0.78	4.4	92	−20	0.006	9.99	Polyimide	1.57 $\lambda_o \times 1.65\ \lambda_o$	–	Yes
[22]	2.8	1.5	–	–	–	–	–	RT/Duriod 6010	1.57 $\lambda_o \times 1.57\ \lambda_o$	–	No
[23]	1.89	1.59	4.60	74.5	−25	15.6×10^{-10}	≈10	SiO_2	0.59 $\lambda_o \times 0.39\ \lambda_o$	–	No
[24]	2.3, 3.2, 4.5	0.038, 0.043, 0.06	>5	>60	>−15	<0.2	9.99	Polyimide	0.78 $\lambda_o \times 0.63\ \lambda_o$	1×2	No
Proposed	4.73, 5.47	1.83	13.15	91.33	−31.41	0.00027	9.9988	Polyimide	1.419 $\lambda_o \times 3.78\ \lambda_o$	1×2	Yes

A. Novelty of the Proposed Antenna Design

The novelty of the proposed antenna design lies in the methodology, architectural solution, and modeling technique, which enable high performance, compact size, and optimal bandwidth for THz communication systems and 6G networks through the integration of an RLC model. The key features of the proposed antenna design are summarized as follows:

- High performance: The antenna achieves a gain of 13.15 dB, 91.33% radiation efficiency, and −31.41 dB isolation, outperforming existing designs in the THz range.
- Compact size: With a footprint of 90 × 205 μm², the antenna is suitable for space-constrained applications.
- Resonance and bandwidth: It operates over a 1.83 THz bandwidth with dual resonance frequencies at 4.73 THz and 5.47 THz, offering significantly improved bandwidth compared to existing designs.
- RLC model integration: The RLC model enhances resonance, impedance matching, and bandwidth optimization, improving efficiency and performance.
- Design strategy and architectural choices: The antenna uses a 2-port MIMO architecture, improving DG and signal quality while maintaining compactness and high efficiency. Additionally, the design incorporates concentric slots to further optimize performance, improve resonance, and minimize interference.
- Modeling approach: Multiple simulation tools, including HFSS, FEKO, CST Studio Suite, and ADS, were used for design validation, ensuring robustness and reliability across different THz bands. The multi-tool validation increases confidence in the design's performance.

II. SINGLE-ELEMENT ANTENNA

The design of the proposed single-element antenna commences with a systematic approach to characterize and optimize its performance. This procedure, governed by a set of design equations, relies on precise material parameters and electromagnetic principles to achieve optimal dimensions. The patch dimensions are determined using the following equations [25]:

$$\lambda = \frac{c}{f} \quad (1)$$

$$\varepsilon_{eff} = \left(\frac{\varepsilon_r+1}{2} + \frac{\varepsilon_r-1}{2}\right) \times \left(1 + 12 \times \frac{h}{W}\right)^{-0.5} \quad (2)$$

$$W = \frac{c}{2f} \times \sqrt{\frac{2}{\varepsilon_r+1}} \quad (3)$$

$$L = \frac{c}{(2f\sqrt{(\varepsilon_{eff})})} - 2 \times \Delta L \quad (4)$$

$$\Delta L = 0.412\, h \times \frac{\frac{\varepsilon_{eff}+0.3}{\frac{w}{h}+0.264}}{\frac{2}{\varepsilon_{eff}-0.258}} \quad (5)$$

Equation (1) defines λ as the wavelength, where c is the speed of light (3×10^8 m/s) and f is the operating resonance frequency. The effective dielectric constant ε_{eff} and the h/W ratio (ε_r = 3.5 for polyimide) are defined in (2), which characterizes wave propagation in the substrate. The patch width W, given in (3), is optimized to achieve proper impedance matching and minimal reflection loss. The patch length (L) is calculated using (4), whereas (5) accounts for fringing field effects to obtain the effective length correction ΔL.

These equations ensure accurate antenna design and optimized electromagnetic performance. The antenna is developed as a single-element structure targeting high efficiency and stable radiation characteristics. At this stage, material selection and substrate thickness are optimized to enhance electrical conductivity, mechanical flexibility, and signal transmission efficiency.

Copper and polyimide are selected due to their favorable properties at THz frequencies. Copper provides high electrical conductivity (~5.8×10^7 S/m), ensuring efficient current flow. However, at THz frequencies, the skin effect confines current to a thin surface layer, increasing effective losses. The polyimide substrate is chosen for its low dielectric loss and mechanical flexibility, making it suitable for high-frequency applications. Even though copper has low dielectric loss, attenuation can still occur. Although copper exhibits low intrinsic loss, overall attenuation is influenced by skin depth effects and substrate properties [26].

As shown in Figure 1, the proposed antenna has a compact footprint of 80 × 90 μm², making it suitable for high-frequency communication systems. The main radiating element is a 60 × 60 μm² copper patch, selected due to its high conductivity and favorable electromagnetic properties. The structure consists of a copper patch and a slotted copper ground plane with a thickness of 2.33 μm. The design incorporates two concentric square rings, a V-shaped slot in the patch, and five additional concentric octagonal slots in the ground plane to enhance impedance matching and radiation performance.

Both the patch and ground are made of copper, whereas polyimide is used as the substrate to minimize signal attenuation and improve radiation efficiency. A polyimide substrate with a dielectric constant of 3.5 and a low loss tangent of 0.0027 is used to reduce dielectric losses [27]. Wave propagation is supported through a 3 μm substrate thickness, contributing to stable high-frequency operation. Overall, these design choices enhance antenna performance for next-generation wireless systems, including 6G applications.

The antenna is validated using CST Studio Suite, where its electromagnetic performance is analyzed, confirming its suitability for high-frequency wireless communication systems.

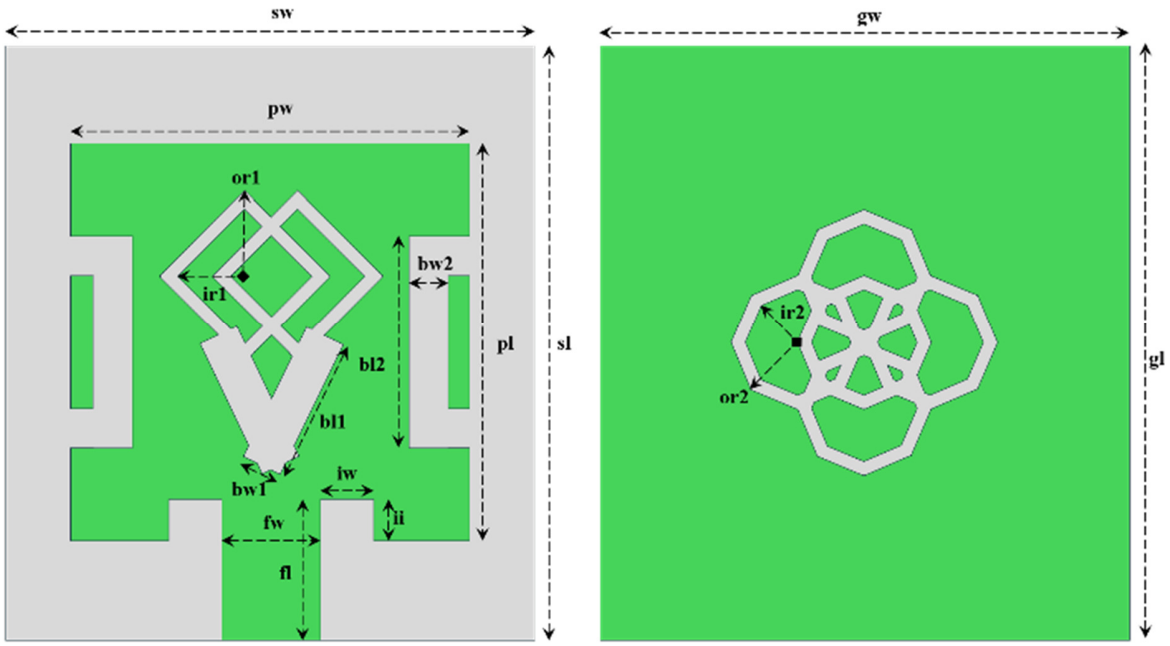

Fig. 1. Front and back view of the single-element antenna.

III. DESIGN METHODOLOGY OF THE SINGLE-ELEMENT ANTENNA

The single-element antenna is optimized through several iterations to achieve the best resonant performance. This process is shown in Figure 2, with the reflection coefficient in Figure 3(a) and the gain in Figure 3(b). The design is improved in each cycle, where a cycle represents one complete simulation-based refinement.

A. Initial Design

The initial antenna is based on a simple modified rectangular patch with two symmetrical inset slots on either side of the feed and two concentric overlapping square slots. However, this structure does not achieve the desired resonant frequency and gain. The input reflection coefficient is low, and the bandwidth is also very small, making the antenna unsuitable for high-performance 6G applications. These results highlight the need for structural modifications to improve both efficiency and bandwidth.

B. Inserting the V-Shaped Slot

In the second stage, a V-shaped slot is introduced under the square slots in the patch to improve resonance and gain. This modification increases both the resonant frequency and gain. The simulated results show one resonant frequency at 4.9 THz, where the bandwidth and gain are slightly improved compared to the first stage. However, the performance is still not sufficient for 6G applications, indicating that further improvement is required.

C. Octagonal Slot on the Ground

The third stage, representing the final proposed element, involves a major redesign to improve antenna performance. Five concentric octagonal slots are introduced in the ground plane to enhance overall efficiency. At this stage, two resonant frequencies are observed at 4.72 THz and 5.96 THz, with corresponding reflection coefficients of −35.6 dB and −37.7 dB. The maximum gain of the proposed design is 10.41 dB, making it a suitable candidate for future high-frequency applications such as 6G.

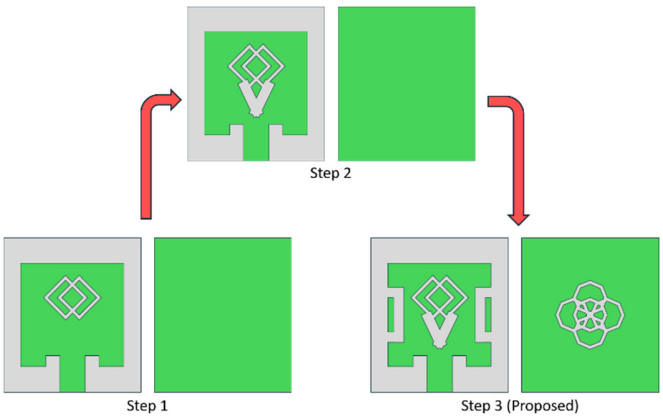

Fig. 2. Evolution of the single-element antenna.

The rectangular patch antenna is progressively refined through each design stage. This iterative approach is supported by parameter optimization to achieve the desired resonant frequency, bandwidth, and gain. The optimized antenna dimensions are: sw = 80 µm, sl = 90 µm, pw = 60 µm, pl = 60 µm, fw = 15 µm, and fl = 22 µm. Therefore, the final design can be considered a well-optimized candidate for ultrahigh-frequency wireless systems.

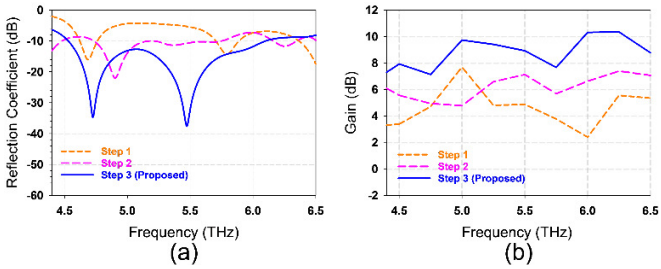

Fig. 3. Design stages of the single-element antenna: (a) reflection coefficient, and (b) gain.

IV. PATCH MATERIAL ANALYSIS

The influence of patch substrate selection on the performance of a microstrip patch antenna is mainly reflected in the operating frequency, gain, and input reflection coefficient. This work compares three different materials, aluminum, copper [28], and graphene [29], to identify the best candidate for THz applications. Their suitability for THz operation is based on their electromagnetic properties and electrical conductivity.

Figure 4(a) shows the simulation results for the reflection coefficient (S11) whereas the antenna gain is shown in Figure 4(b). Initially, aluminum was selected due to its established electrical conductivity and common use in antenna fabrication. The simulation results show that the aluminum patch antenna does not exhibit a clear resonance frequency and has low gain, making it unsuitable for THz applications.

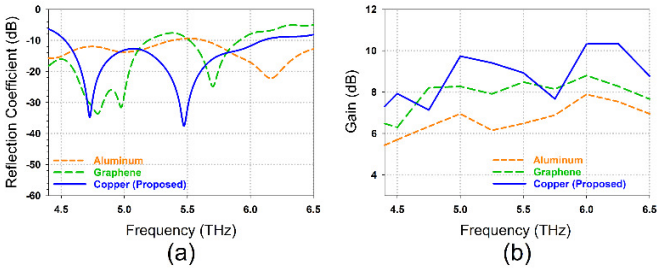

Fig. 4. Comparison of patch materials: (a) reflection coefficient, and (b) gain.

Graphene was also considered as an alternative material [30, 31]. The graphene-based antenna exhibits a single resonance frequency at 5.7 THz with an input reflection coefficient of −25 dB. The operating frequency range is 5.5–5.9 THz; however, graphene is not suitable for broadband THz applications due to its narrow bandwidth and low gain performance.

After evaluating all cases, copper was identified as the best-performing material. The copper-based patch antenna shows two resonant frequencies at 4.72 THz and 5.96 THz, with a maximum gain of 10.41 dB. Copper exhibits a wide bandwidth of 1.59 THz, and its high electrical conductivity and strong electromagnetic response make it suitable for THz applications.

Compared to aluminum and graphene, copper provides better bandwidth and gain performance. Its low-loss characteristics, flexibility, and high radiation efficiency further support its suitability for THz antennas.

This study confirms that copper is the most suitable material for the proposed THz antenna design, outperforming both aluminum and graphene. Its excellent electrical properties enable efficient high-frequency operation, making it a strong candidate for future communication and sensing applications.

V. PARAMETRIC ANALYSIS OF THE SINGLE-ELEMENT ANTENNA

A parametric study of the single-element antenna with respect to patch thickness is presented in this section. The effect of patch thickness on resonance and gain is investigated.

A. Patch Thickness

Variation in patch thickness has a strong influence on antenna performance, as shown in Figure 5. The reflection coefficient is shown in Figure 5(a), and the antenna gain is shown in Figure 5(b). No resonant frequency is observed when the patch thickness is reduced to lower values. For higher thickness values, two resonant frequencies are observed at 4.65 THz and 5.7 THz. However, the −10 dB level is not reached at these frequencies, and therefore no effective bandwidth is obtained. In addition, the gain performance is poor compared to that of the proposed patch thickness.

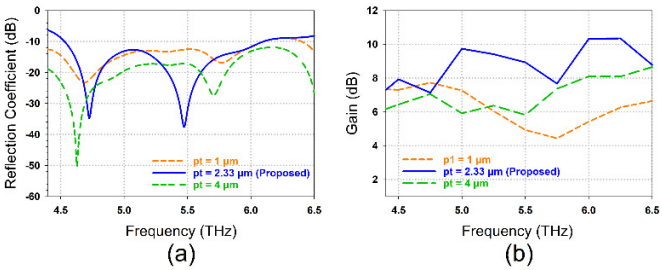

Fig. 5. Effect of patch thickness on antenna performance: (a) reflection coefficient, and (b) gain.

The optimal patch thickness that provides the best compromise among resonant frequency, gain, input reflection coefficient, and bandwidth is 2.33 µm. This value is selected as the optimal solution for the proposed antenna. The results clearly indicate that antenna performance is highly sensitive to variations in patch thickness, highlighting its importance in determining overall performance and efficiency at THz frequencies.

VI. DESIGN AND ANALYSIS OF MIMO ANTENNA

The MIMO technique is considered one of the most promising technologies for future wireless communication systems, particularly for 6G networks [32, 33]. It enables the transmission of multiple data streams, thereby improving system efficiency and robustness. This capability is essential to meet the stringent requirements of 6G applications [34].

This section describes the transformation of a single-element antenna into a dual-port MIMO antenna. Figure 6(a) shows the single-element antenna, whereas the MIMO configuration is presented in Figure 6(b). The two elements are placed side-by-side and separated by 45 µm, forming a compact structure with overall dimensions of 90 × 205 µm². The elements are arranged in a horizontal dual configuration with 180° orientation. This configuration enhances spatial diversity, reduces mutual coupling, and improves signal integrity and reliability.

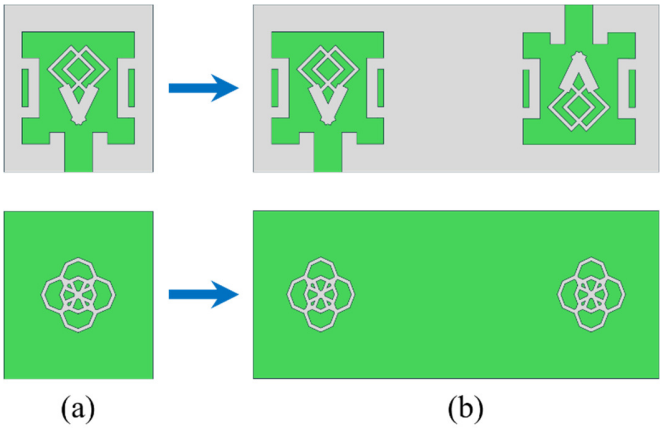

Fig. 6. Proposed antenna configuration: (a) single-element, and (b) MIMO antenna.

The comparison of the input reflection coefficient between the single-element and MIMO antenna, as well as between the two MIMO elements, is shown in Figure 7(a). The MIMO antenna achieves a wide bandwidth with improved input reflection characteristics. Two resonant frequencies are observed at 4.73 THz and 5.47 THz, with a bandwidth of 1.83 THz. This represents a significant improvement compared to the single-element antenna. Although the resonant frequencies remain close, the MIMO configuration provides better performance at higher frequencies. In addition, the isolation reaches −31.41 dB across the operating bandwidth.

Figure 7(b) shows the gain comparison between the single-element and MIMO antennas. The MIMO antenna achieves a maximum gain of 13.15 dB, whereas the single-element antenna provides a gain of 10.41 dB. This gain enhancement highlights the practical potential of the proposed MIMO antenna for future communication systems and high-resolution THz imaging applications.

The optimized antenna dimensions are as follows: sw = 205 µm, sl = 90 µm, st = 3 µm, gw = 205 µm, gl = 90 µm, gt = 2.33 µm, pl = 60 µm, pw = 60 µm, iw = 8 µm, il = 6 µm, b1w = 6 µm, fw = 15 µm, D = 45 µm, b1l = 22 µm, cys2 = 4 µm, cys3 = 8 µm.

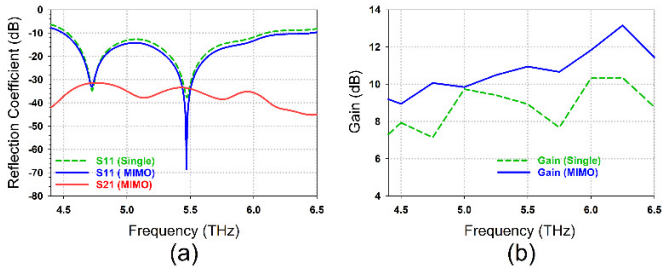

Fig. 7. Proposed MIMO antenna: (a) reflection and transmission coefficients, and (b) gain.

VII. PERFORMANCE ANALYSIS OF THE PROPOSED MIMO ANTENNA

In this section, a comprehensive analysis of the proposed MIMO antenna is presented, covering key performance parameters such as reflection coefficient, transmission coefficient, gain, efficiency, ECC, DG, Channel Capacity Loss (CCL) and Total Active Reflection Coefficient (TARC). The study highlights the antenna's excellent performance and its potential for application in ultra-sensitive THz communication systems.

A. Reflection Coefficient Analysis

The power reflected from an antenna is an important consideration in antenna design, and the input reflection coefficient (S11) is one of the most important parameters in antenna characterization [35]. As shown in Figure 7(a), the reflection coefficient of the proposed antenna exhibits two well-defined resonant frequencies. These occur at 4.73 THz with an input reflection coefficient of −34 dB and at 5.47 THz with an input reflection coefficient of −69 dB. A bandwidth of 1.83 THz is achieved over the 4.5–6.33 THz range. These results demonstrate excellent antenna performance, particularly at high frequencies. The low reflection coefficient values at both resonances indicate efficient radiation and good impedance matching.

To ensure accuracy, the antenna is also simulated using two additional full-wave electromagnetic solvers, HFSS and FEKO, and the results are compared. The reflection coefficient (S11) obtained from CST (solid blue line), HFSS (dashed green line), and FEKO (dashed red line) is shown in Figure 8.

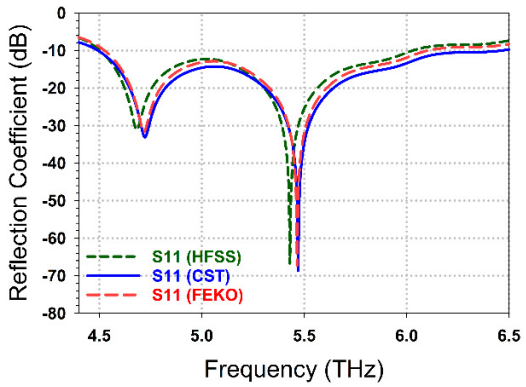

Fig. 8. Reflection coefficient comparison using different simulation software.

The results from all three platforms show strong agreement, demonstrating the consistency and reliability of the simulations. This cross-validation enhances confidence in the proposed antenna design and its performance across different modeling tools.

B. Transmission Coefficient

The transmission coefficient (S21 or S12) represents the power transferred from one antenna element to another. The isolation of the proposed MIMO antenna is −31.41 dB, as shown in Figure 7(a). A lower transmission coefficient (i.e., a more negative dB value) indicates better isolation between the antenna elements. The high isolation achieved in this design demonstrates effective decoupling between the two antenna elements with minimal interference, leading to improved overall system performance [36].

C. Gain and Efficiency

Gain represents how effectively an antenna directs radio-frequency energy in a specific direction, whereas efficiency describes how effectively the antenna converts input power into radiated power [37]. The simulated gain and efficiency of the proposed antenna are presented in Figure 9.

The antenna exhibits high gain and efficiency, making it suitable for high-performance applications. It achieves a peak gain of 13.15 dB over the operating frequency band, indicating effective radiation focusing. This characteristic is important for long-range communication and high-resolution THz imaging [38].

Furthermore, the antenna achieves a radiation efficiency of 91.33% across the operating bandwidth. Higher efficiency values indicate that minimal power is dissipated within the antenna and that most of the input power is effectively radiated.

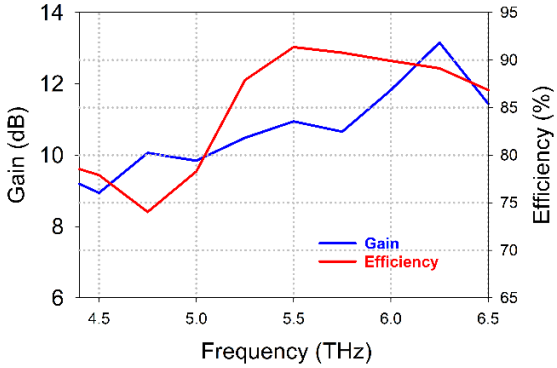

Fig. 9. Gain and efficiency of the proposed MIMO antenna.

D. Envelope Correlation Coefficient

The ECC is a measure of the correlation between the signals received or transmitted by different antenna elements. The ECC value can be computed using the following equation [39]:

$$ECC = \frac{\left|\int_{4\pi}[E_1(\theta,\varphi)*E_2(\theta,\varphi)]d\Omega\right|^2}{\int_{4\pi}|E_1(\theta,\varphi|^2 d\Omega \int_{4\pi}|E_2(\theta,\varphi|^2 d\Omega} \quad (6)$$

The complex electric field distributions of the two antenna elements are denoted by $E_1(\theta, \varphi)$ and $E_2(\theta, \varphi)$, where θ and φ

represent the elevation and azimuth angles, respectively. The solid angle Ω represents the spherical domain, and dΩ is an infinitesimal solid angle element. The integrations are performed over the entire sphere (4π). Figure 10 shows that the proposed antenna has a very low ECC value of 0.00027, which indicates excellent diversity performance. A low ECC reduces signal correlation between antenna elements, minimizing fading and improving system reliability.

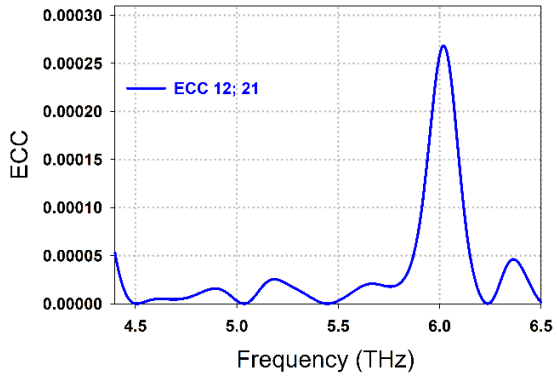

Fig. 10. ECC of the proposed MIMO antenna.

E. Diversity Gain

DG represents the improvement in signal quality achieved through diversity. The value of DG can be determined using the following equation [40]:

$$DG = 10\sqrt{1 - ECC^2} \quad (7)$$

The calculated DG value is 9.9988, which is very close to the ideal value of 10, as shown in Figure 11. A high DG value indicates improved diversity performance and a more reliable communication link.

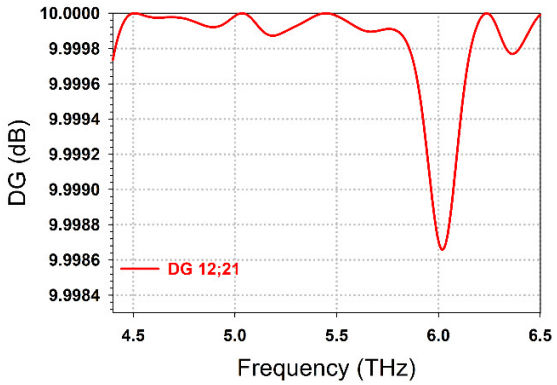

Fig. 11. DG of the proposed MIMO antenna.

F. Total Active Reflection Coefficient

The TARC is an important parameter in MIMO antennas that measures the combined effect of transmitted and received powers, including active components such as matching networks and amplifiers. For efficient antenna performance and low reflected power, the TARC value should be less than 0 dB [41]. Reflected power affects impedance matching, thus proper matching is required to reduce TARC, as reflected signals generate standing waves, reduce efficiency, and increase interference in wireless systems.

$$TARC = \frac{\sqrt{(|S_{xx}|+|S_{xy}|)^2+(|S_{yx}|+|S_{yy}|)^2}}{\sqrt{4}} \quad (8)$$

The proposed MIMO antenna demonstrates excellent performance, with simulated TARC values consistently below −7.7 dB, as shown in Figure 12. These results indicate good impedance matching and very low power reflection.

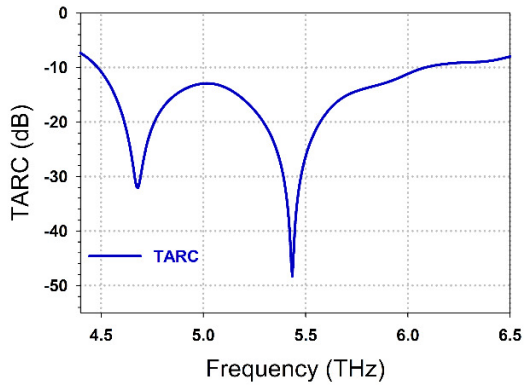

Fig. 12. TARC of the proposed MIMO antenna.

G. Channel Capacity Loss

The performance of MIMO antennas is evaluated using CCL, an important parameter that quantifies the degradation in data transmission efficiency caused by correlation between antenna elements. In ideal MIMO systems, channel capacity is proportional to the number of antennas. However, in practical systems, it is reduced due to mutual coupling and correlation effects. CCL quantifies this reduction and serves as an indicator of MIMO channel efficiency and usability [42]. CCL is calculated using the following equation:

$$CCL = -\log_2 \det(\rho_R) \quad (9)$$

The receiver two-port correlation matrix is defined as:

$$\rho_R = \begin{pmatrix} \rho_{xx} & \rho_{xy} \\ \rho_{yx} & \rho_{yy} \end{pmatrix} \quad (10)$$

where:

$$\rho_{xx} = 1 - \left(|S_{xx}|^2 + |S_{xy}|^2\right)$$

$$\rho_{yy} = 1 - \left(|S_{yy}|^2 + |S_{yx}|^2\right)$$

$$\rho_{xy} = \left|S_{xx}^* S_{xy} + S_{yx}^* S_{xy}\right|^2$$

$$\rho_{yx} = \left|S_{yy}^* S_{yx} + S_{xy}^* S_{yx}\right|^2$$

These parameters describe the interaction between ports 1 and 2 (x and y). For efficient MIMO operation, the CCL should be less than 0.5 bps/Hz. Figure 13 shows that the proposed antenna maintains a CCL of ≤ 0.37 bps/Hz over its operational bandwidth. This low value indicates weak inter-port correlation and confirms efficient MIMO performance.

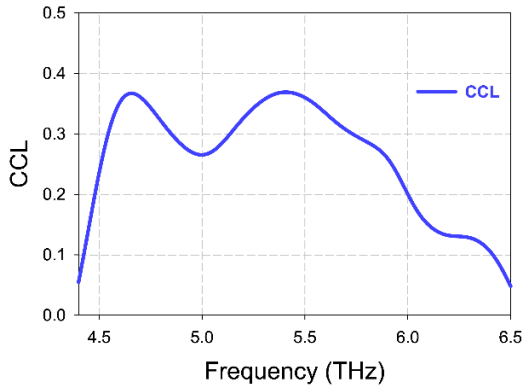

Fig. 13. CCL of the proposed MIMO antenna.

H. Radiation Patterns

E-field and H-field radiation patterns are important parameters for evaluating antenna performance The radiation characteristics of an antenna are strongly influenced by the orthogonality between the fields [43]. As depicted in Figure 14, the E-field and H-field patterns at port 1 of the proposed antenna, excited at the resonant frequency of 5.47 THz, exhibit distinct characteristics. The −3 dB beamwidth of the main lobe of the E-field at port 1 is 36.5°, with a peak amplitude of 17.5 dBV/m at φ = 0°. Meanwhile, the H-field exhibits a magnitude of −33.4 dBA/m with a beamwidth of 32.2°. At φ = 90°, the E-field magnitude is 1.92 dBV/m with a beamwidth of 31.6°, whereas the H-field magnitude is −31.2 dBA/m with a beamwidth of 32.5°. For θ = 90°, the H-field magnitude is −39.7 dBA/m with a beamwidth of 39.5°, whereas the E-field attains a value of 12.2 dBV/m with a beamwidth of 54.7° The radiation pattern analysis also reveals noticeable variations at port 2. At THz frequencies, the antenna exhibits a highly directional beam that is tightly focused in space, as supported by previous studies on E-field and H-field radiation characteristics [30]. Such directional behavior makes the antenna suitable for high-precision wireless communication and sensing applications requiring high-frequency operation.

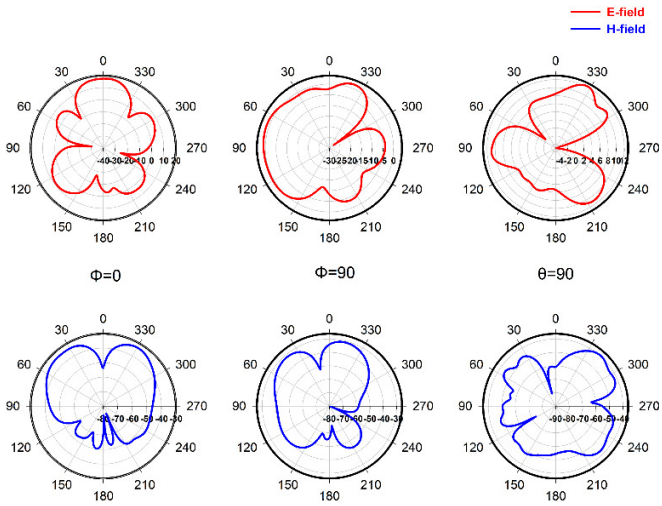

Fig. 14. Radiation patterns of the proposed MIMO antenna.

VIII. RLC EQUIVALENT CIRCUIT

In the pursuit of an advanced antenna design, the proposed antenna is modeled as an RLC circuit, as shown in Figure 15, and its electromagnetic behavior is analyzed. Conventional full-wave electromagnetic simulation tools such as CST Studio Suite are used to extract the equivalent R–L–C parameters from the antenna structure. These parameters are then imported into Agilent ADS for circuit-level simulation and further refinement [44].

The equivalent circuit model is constructed based on the physical structure and electromagnetic behavior of the antenna. The RLC equivalent circuit is developed using a systematic trial-and-error approach in ADS, where the RLC values are tuned iteratively to achieve the desired response. By matching these parameters, the circuit model is made consistent with the antenna's operating frequency characteristics.

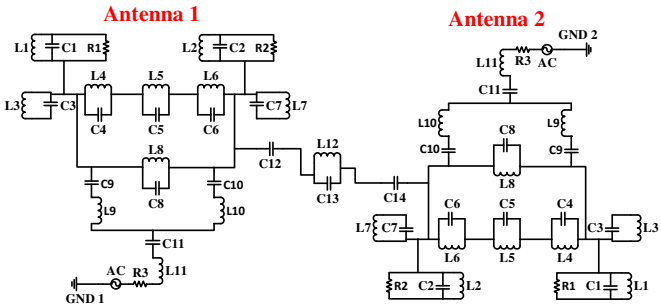

Fig. 15. RLC equivalent circuit of the proposed antenna.

The model consists of a parallel RLC network comprising resistance (R1), inductance (L1), and capacitance (C1), along with an additional parallel branch containing R2, L2, and C2. The left-side slot is modeled using parallel combinations of L3 and C3, whereas the right-side slot is represented using L7 and C7. The left-hand center squares part of the antenna are modeled using parallel RLC groups L4–C4, L5–C5, and L6–C6. The V-shaped slot is represented using L8 and C8. The feedline is modeled using R3, L11, and C11 to replicate its electrical behavior. Fine-tuning of these component values is performed to ensure accurate representation of the antenna's resonant behavior, impedance characteristics, and frequency response.

By combining these lumped elements, a single-element equivalent circuit model is developed that accurately represents the antenna characteristics. Based on this model, a MIMO equivalent circuit is also proposed. The performance of the MIMO antenna is further improved by introducing an additional parallel branch (L12 and C13) to account for mutual coupling effects between antenna elements.

To validate the model, the S11 results obtained from CST simulations are compared with those from the RLC circuit model in ADS. The comparison, shown in Figure 16, demonstrates strong agreement between the two results, confirming that the RLC model accurately represents the behavior of the proposed antenna. The corresponding component values are listed in Table II.

TABLE II. VALUES OF RLC COMPONENTS

Parameter	Value	Parameter	Value	Parameter	Value
L1	6.83 pH	C5	8.78 pF	L3	6.333 pH
C1	3.12 pF	L11	9.44 pH	L8	5.05 pH
R1	50.17 Ω	C6	5.94 pF	C4	9.12 pF
L2	3.51 pH	L12	4.76 pH	L7	3.61 pH
C2	7.57 pF	C7	9.23 pF	C12	5.035 pF
R2	49.19 Ω	L13	8.94 pH	C10	1.34 pF
L5	8.45 pH	C8	4.25 pF	L6	5.51 pH
C3	9.85 pF	L9	6.64 pH	R3	51.25 Ω

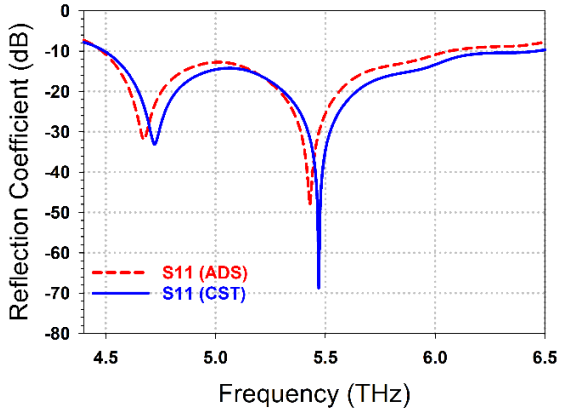

Fig. 16. Comparison of S11 results from ADS and CST for the proposed antenna.

IX. PRACTICAL FEASIBILITY AND LIMITATIONS AT THZ FREQUENCIES

At the very high THz frequencies of 4.73 THz and 5.47 THz, several practical limitations arise due to material properties, fabrication tolerances, and measurement constraints, all of which are critical considerations for real-world antenna implementation.

Material dispersion and skin-depth effects become significant at THz frequencies. The surface conductivity of copper is frequency-dependent due to the skin effect, where the reduced penetration depth leads to increased surface losses and, consequently, a potential reduction in antenna efficiency. These frequency-dependent material properties are incorporated into the simulations to ensure a realistic representation of antenna performance and to support an optimized design. Although copper offers high conductivity, the skin-depth effect still influences overall performance and has therefore been carefully accounted for to minimize its impact.

Fabrication at these dimensions also presents significant challenges. Even minor manufacturing imperfections can lead to noticeable shifts in resonance frequency, bandwidth, and radiation efficiency. To achieve high precision, techniques such as Electron Beam Lithography (EBL) and photolithography are typically required. However, fabrication at the proposed scale remains beyond the capability of most current experimental setups; therefore, this work is primarily simulation-based. Experimental realization will be feasible once the necessary fabrication infrastructure becomes available.

Furthermore, experimental validation at these THz frequencies is currently limited due to the lack of widely available measurement facilities. The high cost and limited accessibility of THz equipment make physical testing challenging at this stage.

X. CONCLUSION

This work demonstrates that the compact high-gain Multiple-Input Multiple-Output (MIMO) antenna operating in the terahertz (THz) band is a strong candidate for sixth-generation (6G) wireless communication systems. The proposed antenna operates at dual resonance frequencies of 4.73 THz and 5.47 THz, covering a maximum bandwidth of 1.83 THz. It achieves a port isolation of −31.41 dB, radiation efficiency of 91.33%, and gain of 13.15 dB, demonstrating excellent overall performance.

The antenna also exhibits superior diversity performance, with an Envelope Correlation Coefficient (ECC) of 0.00027 and a Diversity Gain (DG) of 9.9988 dB, ensuring highly reliable MIMO operation. In addition, the development and validation of the equivalent RLC circuit model provide a reliable framework for performance prediction and further design optimization. The inclusion of the RLC network enhances the antenna's flexibility and ensures stable operation across a wide frequency range.

Owing to its compact size and strong electromagnetic performance, the proposed antenna is well suited for ultra-broadband THz applications, including the Internet of Everything (IoE), 6G communications, and high-resolution imaging systems. Therefore, this work represents a significant advancement in THz antenna design and contributes to the realization of power-efficient, high-data-rate, and low-latency wireless communication systems for future-generation technologies.

DECLARATION OF COMPETING INTERESTS

All authors declare no conflicts of interest.

ACKNOWLEDGMENT

The authors gratefully acknowledge the support provided by Multimedia University, Malaysia and Daffodil International University, Bangladesh.

DATA AVAILABILITY

The datasets generated and/or analyzed during the current study are available from the corresponding author upon reasonable request.

REFERENCES

[1] P. Tiwari, V. Gahlaut, M. Kaushik, P. Rani, A. Shastri, and B. Singh, "Advancing 5G Connectivity: A Comprehensive Review of MIMO Antennas for 5G Applications," *International Journal of Antennas and Propagation*, vol. 2023, no. 1, Aug. 2023, Art. no. 5906721, https://doi.org/10.1155/2023/5906721.

[2] H. Vettikalladi, W. T. Sethi, A. F. B. Abas, W. Ko, M. A. Alkanhal, and M. Himdi, "Sub-THz Antenna for High-Speed Wireless Communication Systems," *International Journal of Antennas and Propagation*, vol. 2019, no. 1, Mar. 2019, Art. no. 9573647, https://doi.org/10.1155/2019/9573647.

[3] R. Chataut, M. Nankya, and R. Akl, "6G Networks and the AI Revolution—Exploring Technologies, Applications, and Emerging Challenges," *Sensors*, vol. 24, no. 6, Mar. 2024, Art. no. 1888, https://doi.org/10.3390/s24061888.

[4] H.-J. Song and N. Lee, "Terahertz Communications: Challenges in the Next Decade," *IEEE Transactions on Terahertz Science and Technology*, vol. 12, no. 2, pp. 105–117, Mar. 2022, https://doi.org/10.1109/TTHZ.2021.3128677.

[5] M. A. Jamshed, A. Nauman, M. A. B. Abbasi, and S. W. Kim, "Antenna Selection and Designing for THz Applications: Suitability and Performance Evaluation: A Survey," *IEEE Access*, vol. 8, pp. 113246–113261, 2020, https://doi.org/10.1109/ACCESS.2020.3002989.

[6] M. F. Ali, R. Bhattacharya, and G. Varshney, "Tunable four-port MIMO/self-multiplexing THz graphene patch antenna with high isolation," *Optical and Quantum Electronics*, vol. 54, no. 12, Oct. 2022, Art. no. 822, https://doi.org/10.1007/s11082-022-04200-x.

[7] O. A. Amodu, C. Jarray, S. A. Busari, and M. Othman, "THz-enabled UAV communications: Motivations, results, applications, challenges, and future considerations," *Ad Hoc Networks*, vol. 140, Mar. 2023, Art. no. 103073, https://doi.org/10.1016/j.adhoc.2022.103073.

[8] P. Das, "Beam-steering of THz MIMO antenna using graphene-based intelligent reflective surface," *Optical and Quantum Electronics*, vol. 55, no. 8, June 2023, Art. no. 711, https://doi.org/10.1007/s11082-023-04996-2.

[9] N. Kiani, F. Tavakkol Hamedani, and P. Rezaei, "Graphene-Based Quad-Port MIMO Reconfigurable Antennas for THz Applications," *Silicon*, vol. 16, no. 9, pp. 3641–3655, June 2024, https://doi.org/10.1007/s12633-024-02939-4.

[10] M. Abd Elaziz *et al.*, "Evolution toward intelligent communications: Impact of deep learning applications on the future of 6G technology," *WIREs Data Mining and Knowledge Discovery*, vol. 14, no. 1, Jan. 2024, Art. no. e1521, https://doi.org/10.1002/widm.1521.

[11] O. A. Amodu, S. A. Busari, and M. Othman, "Physical layer aspects of terahertz-enabled UAV communications: Challenges and opportunities," *Vehicular Communications*, vol. 38, Dec. 2022, Art. no. 100540, https://doi.org/10.1016/j.vehcom.2022.100540.

[12] M. H. Maktoomi, Z. Wang, H. Wang, S. Saadat, P. Heydari, and H. Aghasi, "A Sub-Terahertz Wideband Stacked-Patch Antenna on a Flexible Printed Circuit for 6G Applications," *IEEE Transactions on Antennas and Propagation*, vol. 70, no. 11, pp. 10047–10061, Nov. 2022, https://doi.org/10.1109/TAP.2022.3185497.

[13] Y. Amraoui, I. Halkhams, R. E. Alami, M. O. Jamil, and H. Qjidaa, "High isolation integrated four-port MIMO Antenna for terahertz communication," *Results in Engineering*, vol. 26, June 2025, Art. no. 105253, https://doi.org/10.1016/j.rineng.2025.105253.

[14] Y. Amraoui, I. Halkhams, R. E. Alami, M. O. Jamil, and H. Qjidaa, "High gain MIMO antenna with multiband characterization for terahertz applications," *Scientific African*, vol. 26, Dec. 2024, Art. no. e02380, https://doi.org/10.1016/j.sciaf.2024.e02380.

[15] Y. Amraoui, I. Halkhams, R. El Alami, M. O. Jamil, and H. Qjidaa, "High isolation MIMO antenna array for multiband terahertz applications," *Results in Engineering*, vol. 23, Sept. 2024, Art. no. 102842, https://doi.org/10.1016/j.rineng.2024.102842.

[16] K. Vasu Babu, S. Das, G. Varshney, G. N. J. Sree, and B. T. P. Madhav, "A micro-scaled graphene-based tree-shaped wideband printed MIMO antenna for terahertz applications," *Journal of Computational Electronics*, vol. 21, no. 1, pp. 289–303, Feb. 2022, https://doi.org/10.1007/s10825-021-01831-3.

[17] R. Pant and L. Malviya, "Terahertz MIMO antenna array for future generation of wireless applications," *Frequenz*, vol. 78, no. 5–6, pp. 271–280, June 2024, https://doi.org/10.1515/freq-2023-0203.

[18] K. V. Babu, S. Das, G. N. J. Sree, B. T. P. Madhav, S. K. K. Patel, and J. Parmar, "Design and optimization of micro-sized wideband fractal MIMO antenna based on characteristic analysis of graphene for terahertz applications," *Optical and Quantum Electronics*, vol. 54, no. 5, Apr. 2022, Art. no. 281, https://doi.org/10.1007/s11082-022-03671-2.

[19] R. H. Abd and H. A. Abdulnabi, "Design of graphene-based multi-input multi-output antenna for 6G/IoT applications," *Indonesian Journal of Electrical Engineering and Computer Science*, vol. 31, no. 1, pp. 212–221, July 2023, https://doi.org/10.11591/ijeecs.v31.i1.pp212-221.

[20] A. A. Ibrahim and S. M. Gaber, "Frequency reconfigurable antipodal Vivaldi 2-port antenna based on graphene for terahertz communications," *Optical and Quantum Electronics*, vol. 55, no. 9, June 2023, Art. no. 786, https://doi.org/10.1007/s11082-023-05036-9.

[21] A. Kumar, D. Saxena, P. Jha, and N. Sharma, "Compact two-port antenna with high isolation based on the defected ground for THz communication," *Results in Optics*, vol. 13, Dec. 2023, Art. no. 100522, https://doi.org/10.1016/j.rio.2023.100522.

[22] R. Jain, V. V. Thakare, and P. K. Singhal, "Design and Comparative Analysis of THz Antenna through Machine Learning for 6G Connectivity," *IEEE Latin America Transactions*, vol. 22, no. 2, pp. 82–91, Feb. 2024, https://doi.org/10.1109/TLA.2024.10412032.

[23] K. V. Babu, G. N. J. Sree, T. Islam, S. Das, M. E. Ghzaoui, and R. A. Saravanan, "Performance Analysis of a Photonic Crystals Embedded Wideband (1.41–3.0 THz) Fractal MIMO Antenna Over SiO2 Substrate for Terahertz Band Applications," *Silicon*, vol. 15, no. 18, pp. 7823–7836, Dec. 2023, https://doi.org/10.1007/s12633-023-02622-0.

[24] K. Vijayalakshmi, C. S. K. Selvi, and B. Sapna, "Novel tri-band series fed microstrip antenna array for THz MIMO communications," *Optical and Quantum Electronics*, vol. 53, no. 7, July 2021, Art. no. 395, https://doi.org/10.1007/s11082-021-03065-w.

[25] M. A. Haque *et al.*, "Predictive modelling and high-performance enhancement smart thz antennas for 6 g applications using regression machine learning approaches," *Scientific Reports*, vol. 15, no. 1, Oct. 2025, Art. no. 34640, https://doi.org/10.1038/s41598-025-18458-0.

[26] A. Haque, K. Hossain Nahin, J. Jiat Tiang, M. Hasan, N. Singh Sawaran Singh, and A. Kader Jilani, "High-Gain Dielectric Resonator Antenna for 6G Sub-THz Wireless Networks and Terahertz Sensing," *Journal of Communications*, vol. 20, no. 5, pp. 632–639, Oct. 2025, https://doi.org/10.12720/jcm.20.5.632-639.

[27] Z. Pang *et al.*, "Research Advances of Porous Polyimide—Based Composites with Low Dielectric Constant," *Polymers*, vol. 15, no. 16, Aug. 2023, Art. no. 3341, https://doi.org/10.3390/polym15163341.

[28] R. M. Redzuwan, J. Sampe, R. Latif, Z. A. Rhazali, and N. H. M. Yunus, "Performance analysis of tantalum and copper patches in micro-electro-mechanical systems based microstrip patch antennas for 5th generation mmWave applications," *Advances in Science and Technology. Research Journal*, vol. 19, no. 8, pp. 285–295, Aug. 2025, https://doi.org/10.12913/22998624/205744.

[29] D. Correas-Serrano and J. S. Gomez-Diaz, "Graphene-based Antennas for Terahertz Systems: A Review." arXiv, Apr. 10, 2017, https://doi.org/10.48550/arXiv.1704.00371.

[30] E. P. de Santana *et al.*, "A THz graphene-on-hBN stack patch antenna for future 6G communications," *Scientific Reports*, vol. 15, no. 1, Sept. 2025, Art. no. 32650, https://doi.org/10.1038/s41598-025-16695-x.

[31] Y. Amraoui, I. Halkhams, R. El Alami, M. O. Jamil, and H. Qjidaa, "A Graphene-based multiband MIMO antenna for high performance terahertz applications," *Physica Scripta*, vol. 100, no. 7, June 2025, Art. no. 075023, https://doi.org/10.1088/1402-4896/ade512.

[32] P. S. Chowdary and S. K. Panda, "Performance Analysis of a Swastika shaped MIMO Antenna for Wireless Communication Applications," *Engineering, Technology & Applied Science Research*, vol. 15, no. 1, pp. 19971–19976, Feb. 2025, https://doi.org/10.48084/etasr.9478.

[33] M. A. Haque *et al.*, "High-performance terahertz MIMO antenna for 6G: Graphene integration and machine learning prediction," *Diamond and Related Materials*, vol. 161, Jan. 2026, Art. no. 113182, https://doi.org/10.1016/j.diamond.2025.113182.

[34] G. C. Alexandropoulos, M. A. Islam, and B. Smida, "Full-Duplex Massive Multiple-Input, Multiple-Output Architectures: Recent Advances, Applications, and Future Directions," *IEEE Vehicular Technology Magazine*, vol. 17, no. 4, pp. 83–91, Dec. 2022, https://doi.org/10.1109/MVT.2022.3211689.

[35] V. Mandrić, S. Rupčić, S. Rimac-Drlje, and I. Baxhaku, "Influence of Dielectric Plate Parameters on the Reflection Coefficient of a Planar Aperture Antenna," *Applied Sciences*, vol. 13, no. 4, Feb. 2023, Art. no. 2544, https://doi.org/10.3390/app13042544.

[36] N. Sheriff, S. K. A. Rahim, H. T. Chattha, and T. K. Geok, "Multiport Single Element Mimo Antenna Systems: A Review," *Sensors*, vol. 23, no. 2, Jan. 2023, Art. no. 747, https://doi.org/10.3390/s23020747.

[37] J.-F. Lin and L. Zhu, "Bandwidth and Gain Enhancement of Patch Antenna Based on Coupling Analysis of Characteristic Modes," *IEEE Transactions on Antennas and Propagation*, vol. 68, no. 11, pp. 7275–7286, Nov. 2020, https://doi.org/10.1109/TAP.2020.2995426.

[38] A. D'Arco *et al.*, "Terahertz continuous wave spectroscopy: a portable advanced method for atmospheric gas sensing," *Optics Express*, vol. 30, no. 11, pp. 19005–19016, May 2022, https://doi.org/10.1364/OE.456022.

[39] S. Sarade and S. Ruikar, "Development of Two UWB Multiband MIMO Antennas with Enhanced Isolation and Cross-Correlation," *Engineering, Technology & Applied Science Research*, vol. 13, no. 1, pp. 9893–9898, Feb. 2023, https://doi.org/10.48084/etasr.5422.

[40] H.-J. Song and T. Nagatsuma, "Present and Future of Terahertz Communications," *IEEE Transactions on Terahertz Science and Technology*, vol. 1, no. 1, pp. 256–263, Sept. 2011, https://doi.org/10.1109/TTHZ.2011.2159552.

[41] X. Wei, J. Lu, Y. Miao, J. Huang, Z. Chen, and G. Liu, "High Isolation MIMO Antenna System for 5G N77/N78/N79 Bands," *Micromachines*, vol. 15, no. 6, May 2024, Art. no. 721, https://doi.org/10.3390/mi15060721.

[42] S. Ahmad *et al.*, "A Compact CPW-Fed Ultra-Wideband Multi-Input-Multi-Output (MIMO) Antenna for Wireless Communication Networks," *IEEE Access*, vol. 10, pp. 25278–25289, 2022, https://doi.org/10.1109/ACCESS.2022.3155762.

[43] Md. A. Rahman, S. S. Al-Bawri, M. T. Islam, M. J. Singh, D. Saha, and Md. A. Haque, "A Compact Multiband Microstrip Antenna Design for 5G IOT and Satellite Communication Applications," in *Proceedings of the 8th International Conference on Space Science and Communication*, Penang, Malaysia, 2023, pp. 125–132, https://doi.org/10.1007/978-981-97-0142-1_13.

[44] J. H. Nirob *et al.*, "Optimized tri-band MIMO antenna design for 6G terahertz applications and future connectivity," *TELKOMNIKA Telecommunication Computing Electronics and Control*, vol. 23, no. 2, p. 553~562, Apr. 2025, https://doi.org/10.12928/TELKOMNIKA.V23I2.26579.